# Journal of Materials Chemistry A

Accepted Manuscript






ROYAL SOCIETY OF CHEMISTRY

www.rsc.org/materialsA

Journal Name

COMMUNICATION

# Flexible electrode for long-life rechargeable sodium-ion batteries: effect of oxygen vacancy in $MoO_{3-x}$

Received 00th January 20xx,
Accepted 00th January 20xx

DOI: 10.1039/x0xx00000x

www.rsc.org/nanoscale

**Yifei Li[a†], Dandan Wang[a†], Qinyou An[a], Bush Ren[a], Yaoguang Rong[a], Yan Yao[a, b]***

**Layered molybdenum trioxide ($MoO_3$) has rarely been studied as a electrode material for sodium ion batteries due to low electronic conductivity and irreversible phase transition. Here we demonstrate $MoO_{3-x}$ with well-controlled oxygen vancacy exhibits near theoretical capacity, excellent rate capability, and 2000 stable cycles with minimal capacity loss. The oxgyen vacancy in $MoO_{3-x}$ is responsible for the two-plateau voltage profile in contrast to the sloping feature observed in α-$MoO_3$. This work highlights the importance of oxygen vacancy in enabling long-life rechargeable sodium-ion batteries.**

The cost of lithium is expected to soar when powering the next generation electric vehicles due to the limited resource, rendering developing low-cost alternatives of lithium ion batteries of great importance.[1] The earth abundance and low cost of raw materials become an unparalleled superiority.[2] In this respect, ubiquitous distribution of sodium in the earth's crust has stimulated extensive research interests towards sodium-ion batteries.[3-6]

Molybdenum oxides have enabled a wide range of applications in gas sensing, catalysts, electronic devices and lubricants due to low cost, resource abundance and nontoxicity. In particular, layered molybdenum trioxide (α-$MoO_3$) has been studied as an attractive electrode in rechargeable lithium-ion batteries due to high theoretical specific capacity of 372 mAh $g^{-1}$, corresponding to two electrons reaction per chemical formula.[7-12] However, the poor cycling stability so far has limited its application as battery electrodes for two reasons. One is the low electronic and ionic conductivity, and the other is irreversible phase transition related to intralayer Li insertion.[7] Strategies were developed in the past to overcome such challenges: (i) nanosizing particle size to reduce the Li ion diffusion distance, (ii) carbon coating to increase the electronic conductivity,[9-13] and (iii) pre-intercalation Li, Na or K ions in layered $MoO_3$ to suppress intralayer Li insertion.[14-17]

Oxygen deficient $MoO_{3-x}$ was reported with fast intercalation and excellent electrochemical performance in lithium-ion batteries.[18] According to Law *et al.*,[19] oxygen vacancies in $MoO_{3-x}$ led to increased electronic conductivity. Goodenough *et al.* showed the reduced $MoO_2$ had metallic conductivity as Mo 4d orbitals splitted into $t_{2g}$ and $e_g$ orbitals and one extra electron per metal cation in $MoO_2$ partially populated the higher t bands.[20] Therefore, partially reduced $MoO_{3-x}$ is beneficial for electrochemical applications.[21-24] To the best of our knowledge, $MoO_{3-x}$ so far has not been investigated as an electrode material in sodium-ion batteries.

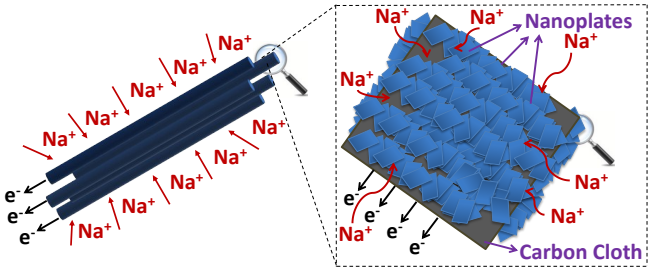


**Fig. 1** Schematic of partial-reduced $MoO_{3-x}$ deposited on flexible carbon cloth to enable facile ion diffusion and electron conduction.

In this work, we demonstrate partially reduced $MoO_{3-x}$ grown on flexible carbon cloth and investigate its electrochemical performance as a sodium-ion electrode material (Fig. 1), exploiting the reducing power of carbon cloth when heated with $MoO_3$. The electrochemical characterizations reveal improved electrochemical performance with a reversible capacity close to theoretical specific capacity of $MoO_3$ (156.3 mAh $g^{-1}$) as well as significantly improved cycling stability (92% capacity retention after 2000 cycles at 1000 mA $g^{-1}$).

To study the effect of oxygen vacancy in $MoO_{3-x}$, Samples 1-3 were prepared as following. Carbon cloth (Fuel Cell Earth CCP40) was cleaned and punched with 1 cm in diameter as. Sample 1 was prepared by annealing the carbon cloth and 0.2 g $MoO_3$ powder in a corundum crucible at 690 °C for 30 min. Molybdenum oxide was deposited on carbon cloth and became partially reduced (~5 mg). Sample 2 was prepared by annealing Sample 1 at 350 °C for 2 h in air. Sample 3 was prepared by annealing Sample 1 at a higher temperature of 450 °C for 2 h in air. All samples were characterized by X-ray diffraction (XRD, Rigaku MiniFlex 600) using Cu Kα radiation (λ = 1.5406 Å), X-ray photoelectron spectroscopy (XPS, VG MultiLab 2000), and scanning electron microscopy (SEM; Gemini LEO 1525).

[a] *Department of Electrical and Computer Engineering and Materials Science and Engineering Program,* [b] *Texas Center for Superconductivity (TcSUH), University of Houston, Houston, Texas, 77204, USA.*

*E-mail: yyao4@uh.edu.*

† *These authors contribute equally to this work.*

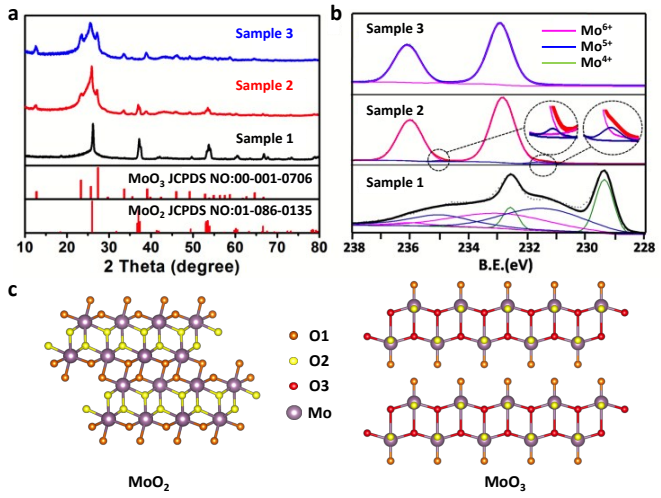


**Fig. 2** (a) XRD patterns of Sample 1-3 and standard PDFs for monoclinic $MoO_2$ and orthorhombic $MoO_3$. (b) XPS of Sample 1, 2 and 3. (c) Crystal structure of $MoO_2$ and α-$MoO_3$ with different oxygen atoms highlighted.

Fig. 2a shows the XRD patterns of Sample 1-3 as well as $MoO_2$ and $MoO_3$ standards. Monoclinic $MoO_2$ (JCPDS No.01-086-0135, a = 5.6096 Å, b = 4.8570 Å, c = 5.6259 Å and β = 120.9120 °) has a distorted rutile structure, which has two O sites labeled as O1 and O2 in Fig. 2c. In comparison, orthorhombic α-$MoO_3$ is a stable bilayered structure (JCPDS No.00-001-0706, a = 3.9540 Å, b = 13.8250 Å, c = 3.6940 Å and α=β=γ=90°) with a space group of Pnma.[25] Each bilayer consists two sublayers of distorted octahedral $MoO_6$ (Fig. 2c). There are three oxygen sites O1, O2 and O3 in the $MoO_3$ structure.[19] O1 oxygen is bonded to one Mo atom, O2 is asymmetrically placed between 2 Mo centers with a two-fold symmetry, while O3 is located among two Mo centers in a sublayer and another Mo center in the neighboring sublayer. Comparing with XRD standards, Sample 1 is mainly monoclinic $MoO_2$ phase, Sample 3 is mainly orthorhombic α-$MoO_3$ phase, while Sample 2 is a mixture of $MoO_3$ and $MoO_2$ phases.

In order to quantify the concentration (x) of oxygen vacancy in $MoO_{3-x}$ samples, we conducted XPS measurements and the results are shown in Fig. 2b and summarized in Table 1. Deconvolution of the Mo 3d spectra in Sample 1 reveals simultaneous existence of peaks of $Mo^{4+}$, $Mo^{5+}$ and $Mo^{6+}$. $Mo^{4+}$ consists of two well-defined peaks located at 229.4 eV for $Mo^{4+}$ $3d_{5/2}$ and 232.6 eV for $Mo^{4+}$ $3d_{3/2}$.[26, 27] Peaks at 235.1 and 231.6 eV for $Mo^{5+}$ and 236.0 and 232.9 eV for $Mo^{6+}$ exist with smaller percentage. Through fitting the peak area ratio in XPS spectra, we obtain the average valence state of Mo in Sample 1 is 5.0 and x is 0.5 in $MoO_{3-x}$. In Sample 2, the peaks corresponding to $Mo^{6+}$ located at 236.0 eV and 232.9 eV become dominant, while $Mo^{5+}$ peaks are suppressed and $Mo^{4+}$ peaks even disappear. The average valence state of Mo in Sample 2 is 5.94 and thus x is 0.03 in $MoO_{3-x}$. In Sample 3, the XPS spectrum shows sharp Mo $3d_{5/2}$ peak at 232.9 eV and Mo $3d_{3/2}$ peak at 236 eV, suggesting x is 0 in Sample 3.[28, 29] Therefore, it is clear that carbon cloth reduces $MoO_3$ to $MoO_{2.5}$ during synthesis; thermal annealing in air partially oxidize Mo back and results in a mixture of $Mo^{5+}$ and $Mo^{6+}$.

Fig. 3a-c show the SEM images of Sample 1-3, in which carbon fibers are clearly visible. At intermediate magnification (Fig. 3d-f), $MoO_{3-x}$ nanoplates uniformly cover the surface of carbon fibers. They are several micrometers in length and a few hundred nanometers in thickness (Fig. 3g-i). The nanosized $MoO_{3-x}$ plates would allow fast kinetics for Na-ion diffusion due to the short diffusion distance. In addition, conductive carbon fiber network retains very well during the annealing process. All three $MoO_{3-x}$ samples show similar nanoscale morphology, therefore allowing us to compare electrochemical performance solely based on the difference of oxygen vacancy in the structure.

**Table 1**. Deconvolution of XPS spectra in Sample 1-3.

| | | Sample 1 | Sample 2 | Sample 3 |
|---|---|---|---|---|
| $Mo^{6+}$ | $3d_{3/2}$ | 260 | 8792 | 5663 |
| | $3d_{5/2}$ | 4700 | 14241 | 8812 |
| $Mo^{5+}$ | $3d_{3/2}$ | 1700 | 440 | 0 |
| | $3d_{5/2}$ | 6600 | 440 | 0 |
| $Mo^{4+}$ | $3d_{3/2}$ | 1300 | 0 | 0 |
| | $3d_{5/2}$ | 3705 | 0 | 0 |
| Valence state | | 5.00 | 5.94 | 6.00 |
| x in $MoO_{3-x}$ | | 0.50 | 0.03 | 0 |

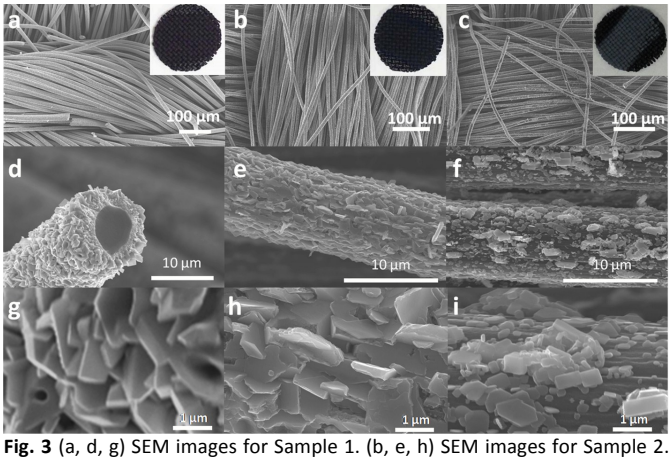


**Fig. 3** (a, d, g) SEM images for Sample 1. (b, e, h) SEM images for Sample 2. (c, f, i) SEM images for Sample 3. Insets show the optical images of Sample 1-3.

To shed light on the effect of oxygen vacancy concentration on electrochemical performance, three samples were measured using CR2032 coin cells with sodium metal as the counter electrode and 1 M $NaClO_4$ in propylene carbonate as the electrolyte. No additional conductive agent or binder is used. Fig. 4a-c display the discharge-charge voltage profiles of three samples at 1st, 50th, and 100th cycle at low rate (current density of 100 mA $g^{-1}$). Sample 1 shows negligible capacity at the first cycle, and slowly increases to ~ 60 mAh $g^{-1}$ after 100 cycles. Interestingly, the voltage profile develops a two-plateau characteristic, which is quite different from the sloping profile typically observed in orthorhombic α-$MoO_3$ after the first cycle.[30] The sloping profile suggests the amorphous structure of α-$MoO_3$ after the first cycle, while plateaus observed in sample 1 indicate the ability of oxygen vacancy to stabilize the crystalline structure of $MoO_{3-x}$ during cycling. Sample 2 also shows a two-voltage plateau but with higher capacity of 156 mAh $g^{-1}$, close to the theoretical specific capacity of $MoO_{3-x}$. For Sample 3, the capacity shows capacity as high as 156 mAh $g^{-1}$ in the first cycle. However only 40% of capacity retention is observed after 50 cycles, which is comparable to the performance of orthorhombic α-$MoO_3$.[10] These results indicate 3% oxygen vacancy (sample 2) is ideal for both high capacity and stable cycling. Too much (sample 1) or too little

(sample 3) oxygen vacancy results in reduced electrochemical performance.

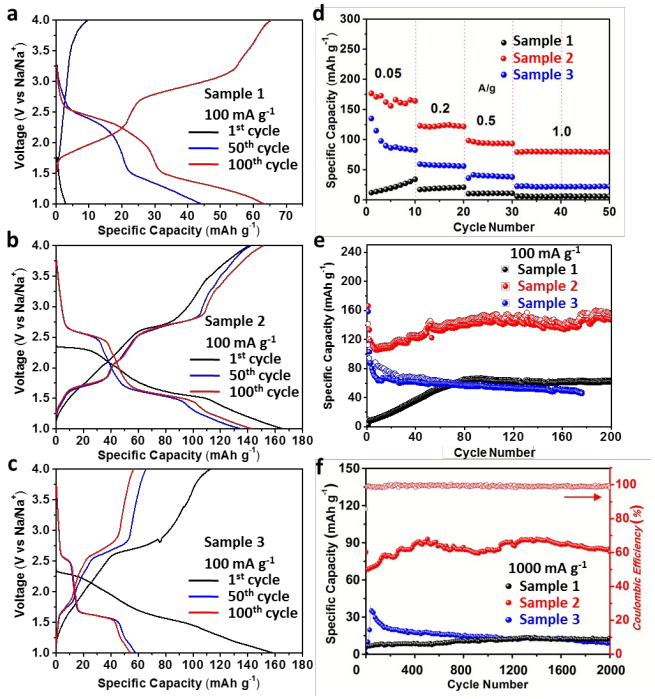


**Fig. 4** (a-c) Galvanostatic charge–discharge profiles of Sample 1-3 at the current of 100 mA $g^{-1}$. (d) The rate performance of Sample 1-3. (e) Cycling performance of Sample 1-3 at the current of 100 mA $g^{-1}$, with discharge and charge capacities. (f) Long-term cycling performance of Sample 1-3 at the current of 1000 mA $g^{-1}$.

The rate capabilities of Sample 1-3 are further tested at various current densities (50 to 1000 mA $g^{-1}$) within the voltage window of 1.0-4.0 V vs $Na/Na^+$ (Fig. 4d). Sample 2 delivers the highest capacity among three samples with its discharge capacity of 176.6, 122.9, 98.4 and 79.2 mAh $g^{-1}$ at current densities of 50, 200, 500 and 1000 mA $g^{-1}$, respectively. Fig. 4e and f show the cycling performance of three samples at 100 and 1000 mA $g^{-1}$, respectively. With an initial capacity drop at 100 mA $g^{-1}$, the capacity of Sample 2 increases over cycling and eventually reaches 156.3 mAh $g^{-1}$ after 200 cycles, corresponding to 0.84 sodium ion per $MoO_{3-X}$. Excellent stability in Sample 2 arises from a balanced mixture of conductive $MoO_2$ phase and Na-intercalating $MoO_3$ phase. Fluctuation in specific capacity during cycling is observed and is possibly due to the uneven electrolyte wetting of two phases of $MoO_2$ and $MoO_3$. This phenomenon has been previously observed in amorphous $MnO_x$-carbon nanocomposites,[31] and in $\alpha$-$Fe_2O_3$/$\beta$-$MnO_2$ nanorods[32] during lithium-ion storage. Sample 1 approaches specific capacity of 64 mAh $g^{-1}$ after 80 cycles. Sample 3 has initial specific capacity of 157 mAh $g^{-1}$, but decays very fast with only 63.4 mAh $g^{-1}$ after 100 cycles. Similar decay is well known for $MoO_3$ in lithium-ion batteries due to the irreversible phase transition and intralayer trapping of Li ions.[8, 33-37] At the current density of 1000 mA $g^{-1}$ (Fig. 4f), Sample 2 still shows the best performance. The discharge capacity of Sample 2 increases to 92.6 mAh $g^{-1}$ after 500 cycles and then shows minimal capacity loss over 2000 cycles, with a 92% capacity retention compared to the capacity at 500th cycle.

## Conclusions

In summary, partially reduced $MoO_{3-x}$ grown on flexible carbon cloth has been synthesized via a facile thermal reduction method. The obtained $MoO_{3-x}$ with well-controlled oxygen vacancies exhibits near theoretical capacity, good rate capability and much enhanced cycling stability. Moreover, it presents very small capacity loss over 2000 cycles at high rate (1000 mA $g^{-1}$). Further investigations of XRD and XPS reveal that the best performing electrode features 3% oxygen vacancy in the structure of $MoO_{3-x}$. This study demonstrates the importance of controlling oxygen vacancy in optimizing materials for long-life rechargeable sodium-ion batteries.

## Acknowledgment

We acknowledge the support from the National Science Foundation (CMMI-1400261).

## Notes and references

1. S.-W. Kim, D.-H. Seo, X. Ma, G. Ceder and K. Kang, *Advanced Energy Materials*, 2012, **2**, 710-721.
2. B. Dunn, H. Kamath and J. M. Tarascon, *Science*, 2011, **334**, 928-935.
3. K. B. Hueso, M. Armand and T. Rojo, *Energy & Environmental Science*, 2013, **6**, 734-749.
4. D. Kundu, E. Talaie, V. Duffort and L. F. Nazar, *Angewandte Chemie International Edition*, 2015, **54**, 3431-3448.
5. S. Li, Y. Dong, L. Xu, X. Xu, L. He and L. Mai, *Advanced Materials*, 2014, **26**, 3545-3553.
6. Y. Li, Y. Liang, F. C. Robles Hernandez, H. Deog Yoo, Q. An and Y. Yao, *Nano Energy*, 2015, **15**, 453-461.
7. X. J. Wang, R. Nesper, C. Villevieille and P. Novák, *Advanced Energy Materials*, 2013, **3**, 606-614.
8. T. Brezesinski, J. Wang, S. H. Tolbert and B. Dunn, *Nat Mater*, 2010, **9**, 146-151.
9. W. Tang, L. Liu, Y. Zhu, H. Sun, Y. Wu and K. Zhu, *Energy & Environmental Science*, 2012, **5**, 6909-6913.
10. M. Baldoni, L. Craco, G. Seifert and S. Leoni, *Journal of Materials Chemistry A*, 2013, **1**, 1778-1784.
11. L. Noerochim, J. Z. Wang, D. Wexler, Z. Chao and H. K. Liu, *Journal of Power Sources*, 2013, **228**, 198-205.
12. W. Tang, Y. Zhu, Y. Hou, L. Liu, Y. Wu, K. P. Loh, H. Zhang and K. Zhu, *Energy & Environmental Science*, 2013, **6**, 2093-2104.
13. Y. Liu, B. H. Zhang, S. Y. Xiao, L. L. Liu, Z. B. Wen and Y. P. Wu, *Electrochimica Acta*, 2014, **116**, 512-517.
14. J. G. Simmons, G. S. Nadkarni and M. C. Lancaster, *Journal of Applied Physics*, 1970, **41**, 538-544.
15. L. Q. Mai, B. Hu, W. Chen, Y. Y. Qi, C. S. Lao, R. S. Yang, Y. Dai and Z. L. Wang, *Advanced Materials*, 2007, **19**, 3712-3716.
16. Y. Dong, X. Xu, S. Li, C. Han, K. Zhao, L. Zhang, C. Niu, Z. Huang and L. Mai, *Nano Energy*, 2015, **15**, 145-152.
17. Z. Hu, C. Zhou, M. Zheng, J. Lu, B. Varghese, H. Cheng and C.-H. Sow, *The Journal of Physical Chemistry C*, 2012, **116**, 3962-3967.

18. P. Meduri, E. Clark, J. H. Kim, E. Dayalan, G. U. Sumanasekera and M. K. Sunkara, *Nano Letters*, 2012, **12**, 1784-1788.
19. D. O. Scanlon, G. W. Watson, D. J. Payne, G. R. Atkinson, R. G. Egdell and D. S. L. Law, *The Journal of Physical Chemistry C*, 2010, **114**, 4636-4645.
20. J. B. Goodenough, *Progress in Solid State Chemistry*, 1971, **5**, 145-399.
21. B. Hu, L. Mai, W. Chen and F. Yang, *ACS Nano*, 2009, **3**, 478-482.
22. Y. Xu, R. Yi, B. Yuan, X. Wu, M. Dunwell, Q. Lin, L. Fei, S. Deng, P. Andersen, D. Wang and H. Luo, *The Journal of Physical Chemistry Letters*, 2012, **3**, 309-314.
23. Y. Shi, B. Guo, S. A. Corr, Q. Shi, Y.-S. Hu, K. R. Heier, L. Chen, R. Seshadri and G. D. Stucky, *Nano Letters*, 2009, **9**, 4215-4220.
24. Y. Sun, X. Hu, W. Luo and Y. Huang, *ACS Nano*, 2011, **5**, 7100-7107.
25. N. A. Chernova, M. Roppolo, A. C. Dillon and M. S. Whittingham, *Journal of Materials Chemistry*, 2009, **19**, 2526-2552.
26. X. Xiao, Z. Peng, C. Chen, C. Zhang, M. Beidaghi, Z. Yang, N. Wu, Y. Huang, L. Miao, Y. Gogotsi and J. Zhou, *Nano Energy*, 2014, **9**, 355-363.
27. J. Światowska-Mrowiecka, S. de Diesbach, V. Maurice, S. Zanna, L. Klein, E. Briand, I. Vickridge and P. Marcus, *The Journal of Physical Chemistry C*, 2008, **112**, 11050-11058.
28. T. H. Fleisch and G. J. Mains, *The Journal of Chemical Physics*, 1982, **76**, 780-786.
29. J. G. Choi and L. T. Thompson, *Applied Surface Science*, 1996, **93**, 143-149.
30. M. E. Spahr, P. Novák, O. Haas and R. Nesper, *Journal of Power Sources*, 1995, **54**, 346-351.
31. J. Guo, Q. Liu, C. Wang and M. R. Zachariah, *Advanced Functional Materials*, 2012, **22**, 803-811.
32. X. Gu, L. Chen, Z. Ju, H. Xu, J. Yang and Y. Qian, *Advanced Functional Materials*, 2013, **23**, 4049-4056.
33. H. Liu, Y. Wang, W. Yang and H. Zhou, *Electrochimica Acta*, 2011, **56**, 1392-1398.
34. F. Tanguy, J. Gaubicher and D. Guyomard, *Electrochimica Acta*, 2010, **55**, 3979-3986.
35. S. Jouanneau, A. Verbaere, S. Lascaud and D. Guyomard, *Solid State Ionics*, 2006, **177**, 311-315.
36. X. Xu, Y.-Z. Luo, L.-Q. Mai, Y.-L. Zhao, Q.-Y. An, L. Xu, F. Hu, L. Zhang and Q.-J. Zhang, *NPG Asia Mater*, 2012, **4**, e20.
37. Q. An, F. Lv, Q. Liu, C. Han, K. Zhao, J. Sheng, Q. Wei, M. Yan and L. Mai, *Nano Letters*, 2014, **14**, 6250-6256.

A long-life sodium ion cathode based on $MoO_{3-x}$ through careful control of oxygen vacancy in MoO3-x exhibits near theoretical capacity, excellent rate capability, and much enhanced cycling stability.